Supporting Information

Modeling the mechanism of CO2/cyclohexene oxide copolymerization catalyzed by chiral zinc β-diiminates: factors affecting reactivity and isotacticity

Huiling Shao*, Yernaidu Reddi, Christopher J. Cramer

Corresponding Author: Huiling Shao (shaoh@umn.edu)

Department of Chemistry, Minnesota Supercomputing Institute and Chemical Theory Center, University of Minnesota, Minneapolis, Minnesota 55455, United States

1. Computational method benchmark of the initiation cycle

We calculated the single point energy of key intermediates and transition states along the cycle of initiation of the C1-catalyzed CHO/CO_2 copolymerization reaction, and the rate-limiting TS1 with catalysts C10 (dichloro substituted) and C11 (dibromo substituted) with different DFT methods and basis set. As illustrated in **Table S1**, we used M06[1] and MN15[2] with a mixed basis set of SDD for Zn and 6-311+G(d,p)

for other atoms. We have also tested ωB97XD with a def2-TZVP[3] basis set. Because the energies calculated with MN15 leads to consistent conclusions on the most favored reaction mechanism and the predicted enantioselectivity, we conclude that our choice of DFT functional in the manuscript is good enough to model this reaction. Noting that although M06 predicted the same enantioselectivity, it failed to describe the exergonic nature of the CHO/CO_2 copolymerization reaction. Moreover, because changing the basis set to def2TZVP had minimal effect on the computed energies, we conclude that our choice of basis set in the manuscript is good enough to model this reaction. The predicted higher enantioselectivity with catalyst C10 and C11 are maintained with different functional and basis sets as well.

TableS1. Benchmark of the computational methods of Zn-catalyzed CHO/CO_2 copolymerization reaction along the cycle of initiation. (All energies are in kcal/mol)

	$SMD_{(toluene)}$/M06/ 6-311+G(d,p)/SDD		$SMD_{(toluene)}$/MN15/ 6-311+G(d,p)/SDD		$SMD_{(toluene)}$/ωb97XD /def2TZVP	
	ΔE	ΔG	ΔE	ΔG	ΔE	ΔG
IM1	0.0	0.0	0.0	0.0	0.0	0.0
IM2	-6.0	9.7	-0.5	10.7	-6.2	9.5
TS1	5.3	21.5	5.5	21.7	4.7	20.9
TS1_*SS*	7.0	24.2	8.0	25.2	8.0	25.2
IM3	-17.0	2.3	-17.9	1.4	-19.6	-0.3
TS2	2.8	31.7	0.1	29.0	2.2	31.1
IM4	-26.2	5.6	-32.8	-1.0	-31.1	0.7
TS1b	7.4	40.5	5.2	38.3	5.2	38.3
IM5	-26.3	9.9	-29.3	7.0	-29.2	7.0
IM6	-7.5	1.2	-6.9	1.7	-7.5	1.1
TS3	-5.3	15.0	-7.2	13.1	-3.8	16.5
IM7	-11.6	11.2	-18.7	4.1	-14.6	8.1
IM8	-58.5	4.7	-71.3	-8.1	-65.4	-2.3
IM1_C10	0.0	0.0	0.0	0.0	0.0	0.0
TS1_RR_C10	-0.9	16.3	2.4	19.6	2.0	19.2
TS1_SS_C10	4.5	22.3	6.7	24.4	7.2	24.9
IM1_C11	0.0	0.0	0.0	0.0	0.0	0.0
TS1_RR_C11	0.0	17.4	3.0	20.4	2.5	19.9
TS1_SS_C11	5.4	23.1	7.9	25.6	8.1	25.9

2. Higher energy conformations of the catalyst resting state

We first investigated the identity of the resting state of catalyst **C1** in the cycle of initiation (**IM1**). As shown in Figure S1, the formation of **IM1** from the original **C1** catalyst is thermodynamically favored by 8.1 kcal/mol. The formation of a potentially inactive catalyst **C1_inactive**, where two BDI ligands bind one Zn-center, is highly unfavorable evidenced by the high activation free energy of 45.6 kcal/mol, with respect to **IM1**. This is likely because of the steric repulsion between bulky ortho *N*-aryl substituents. In the most stable conformation of **IM1 (*dimer-anti*)**, the *N*-aryl groups (colored in yellow) and the *N*-cyclohexyl groups (colored in red and blue) locate on different side of the plane created by the two Zn atoms and the two acetate groups. In the future discussions, whenever the *N*-aryl groups and the *N*-cyclohexyl groups locates on different side of the plane created by the two Zn atoms and the two acetate groups will be called ***dimer-anti***. In **IM1_syn**, the *N*-aryl groups and the *N*-cyclohexyl groups locates on different side of the plane

created by the two Zn atoms and the two acetate groups, and this relative orientation will be called ***dimer-syn***. **IM1_syn** is 18.8 kcal/mol higher in energy with respect to **IM1**.

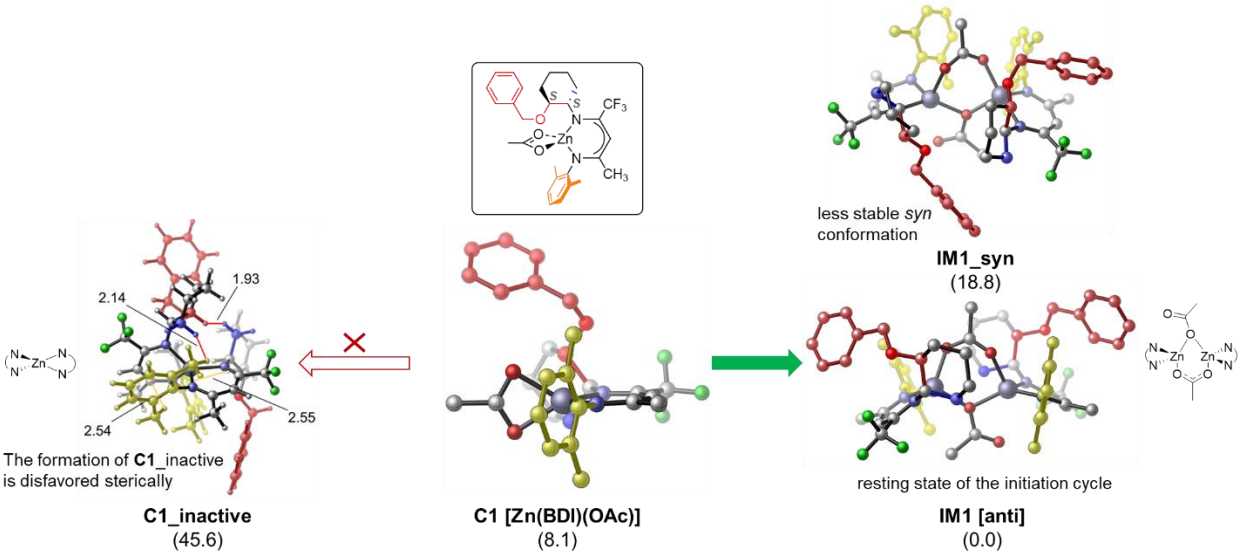

Figure S1. Formation of the resting state (**IM1**) of catalyst **C1** in the cycle of initiation (ΔG in kcal/mol)

The acetate groups can also bridge the Zn-centers in an μ,η^2-fashion (**IM1_8**). Because of the asymmetric nature of the BDI ligand used, the formed dimer compound consequently has four possible conformations (2 degrees of freedom) depending on the orientation of *N*-substituents. On top of the ***dimer-anti*** and ***dimer-syn*** we defined, the relative position of the red part of the *N*-cyclohexyl group and the blue part of the *N*-cyclohexyl group will be identified as ***Cy-anti*** and ***Cy-syn***. Take the lowest energy conformation of **IM1** for example. In **IM1_8_anti_anti**, the two *N*-aryl groups and the two *N*-cyclohexyl groups are on opposite side locate on different side of the plane created by the two Zn atoms (or the *xz* plane). The red part of the left *N*-cyclohexyl group and the red part of the right *N*-cyclohexyl group locate on opposite side of the plane created by the two Zn atoms and the nitrogen atoms of the BDI ligands (or the *xy* plane). Among the four conformations, the **IM1_8_anti_anti** with the longest Zn-Zn separation (4.07Å) is the most stable conformation (7.6 kcal/mol). This conformation has also been observed by Coates in X-ray crystallography studies.[4]

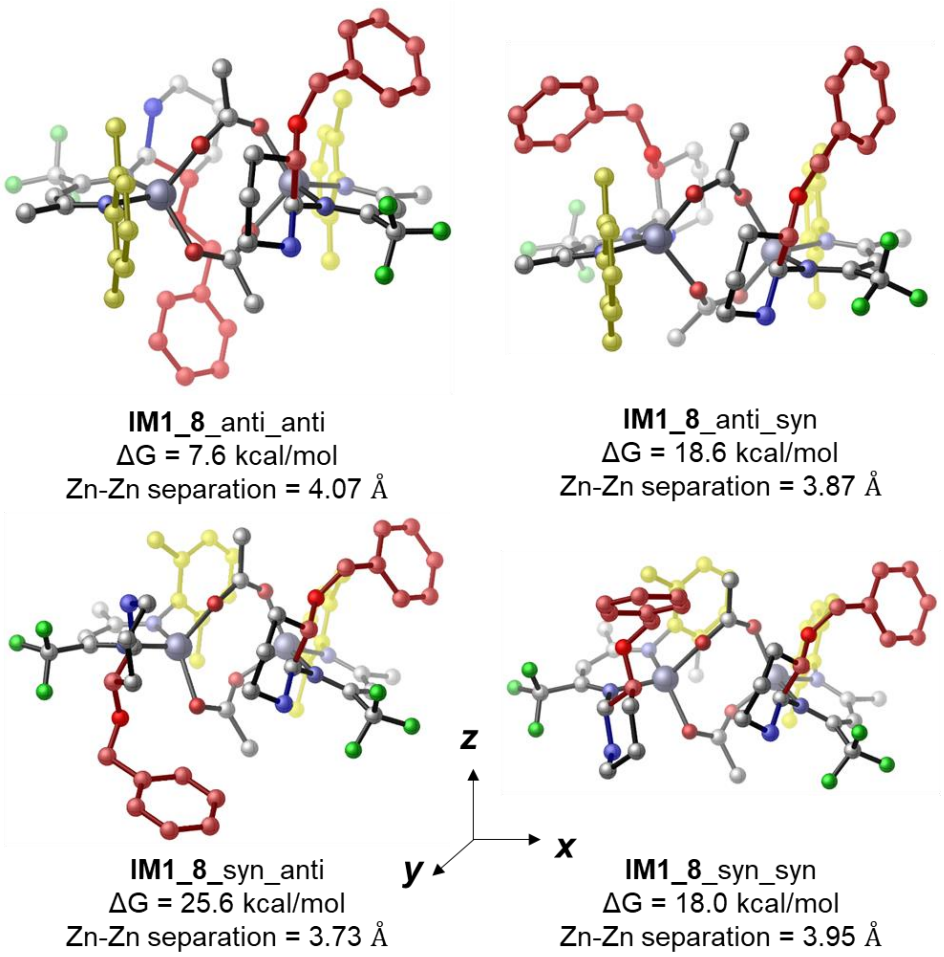

Figure S2. 4 conformations of the **IM1_8** complex with bridging μ,η^2-acetates

3. Higher energy conformations of IM2

The subsequent cyclohexene oxide (CHO) (purple) coordination introduced a third degree of conformational freedom (**Figure S3**). As such, a total of $2^3 = 8$ conformations is available of the **IM2**. In conformations where CHO substrate coordinates to the Zn-atom closer to the red part of the *N*-cyclohexyl substituent (left four conformations), we label them with ***RED***; and in conformations where CHO substrate coordinates to the Zn-atom closer the blue part of the *N*-cyclohexyl substituent (right four conformations), we label them with ***BLUE***. Among the 8 optimized conformations, **IM2** is the lowest energy conformation. In which the relative position of the two BDI ligands is ***Cy-syn*** and ***Cy-anti***, with CHO coordinates to the Zn atom so it is closer to the ***RED*** label.

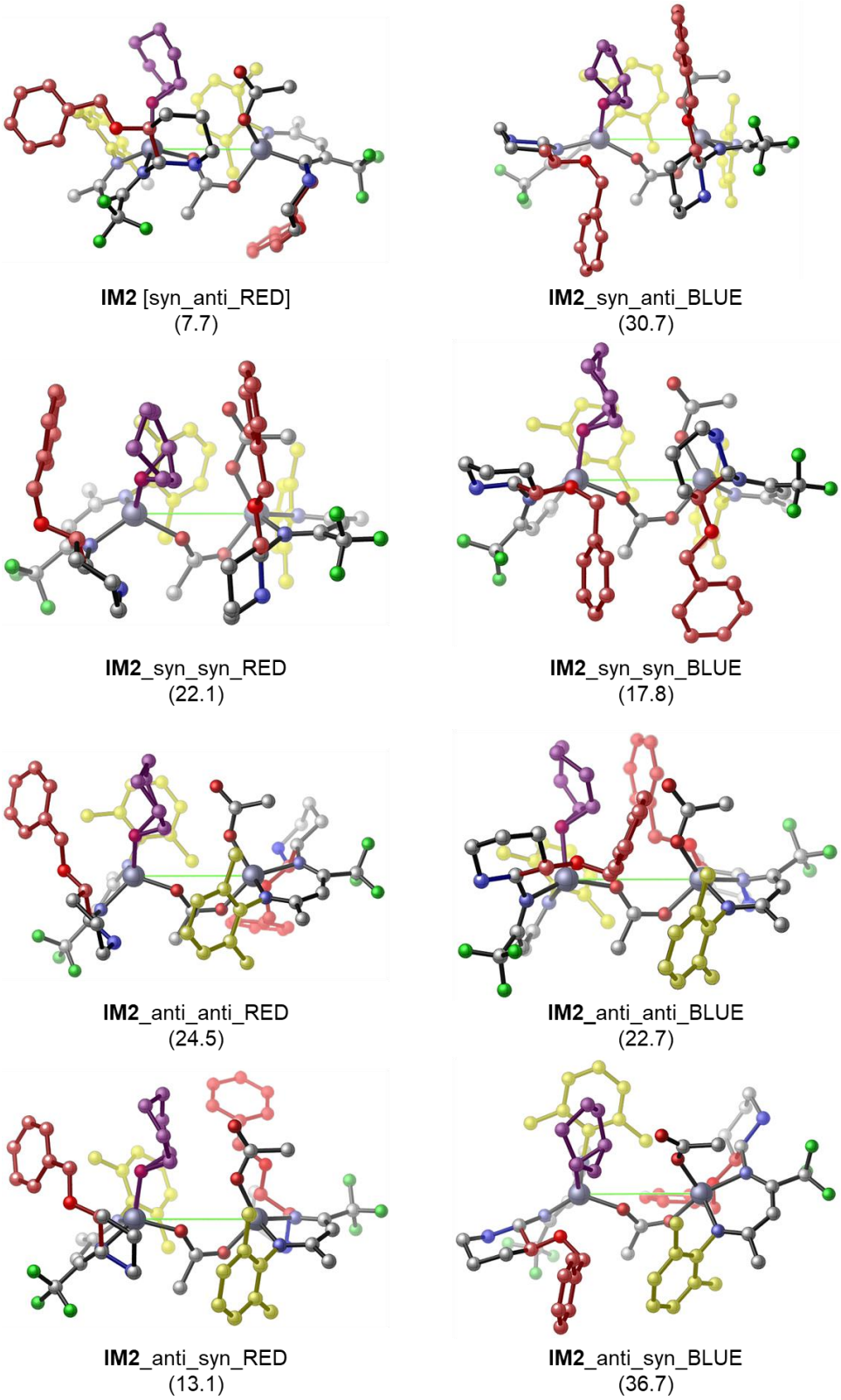

Figure S3. 8 conformations of the CHO coordinated **IM2** (ΔG in kcal/mol)

4. Higher energy conformations of the CHO insertion transition state (TS1) and the Zn-acetate/Zn-alkoxy dimer intermediate (IM3)

On top of the three degrees of freedom we discussed in section 2 and 3, (***dimer-syn*** and ***dimer-anti***; ***CY-syn*** and ***CY-anti; RED*** and ***BLUE***), the CHO ring-opening transition state (**TS1**) has two more degrees of freedom. Firstly, in the ring-opening transition state, the forming C-O bond can face closer to the *N*-cyclohexyl group (***bottom)*** or to the *N*-aryl group (***top*****) (Figure S4)**. Secondly, we can form *R,R* or *S,S* stereocenters after the ring-opening step.

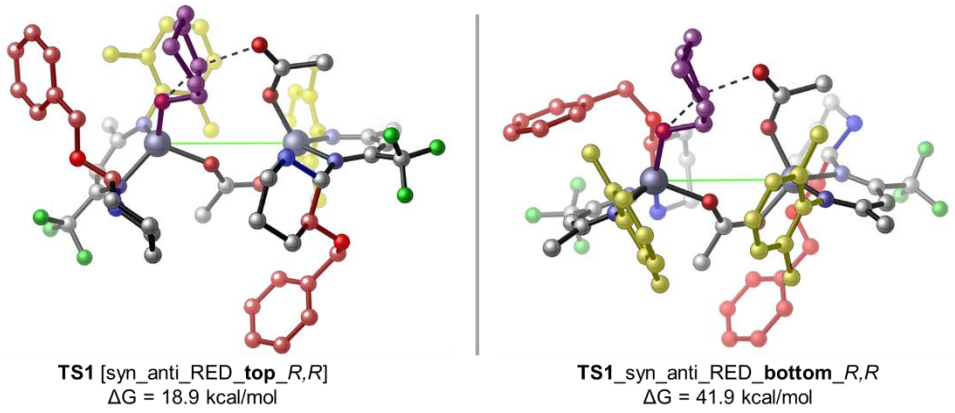

Figure S4. Illustration on the definition of ***top*** and ***bottom*** labels

As such, there are at least a total of 2^5 = 32 conformations (16 of each enantiomers) of **TS1** and the subsequent Zn-acetate/Zn-alkoxy dimer intermediate (**IM3**). The computed activation of free energies is summarized in **Table S2**. The lowest energy conformations of **TS1**_***R,R*** and **TS1**_***S,S*** are entry 10 and 25, respectively.

Table S2. Calculated ΔG‡ of TS1 and IM3 (All energies are calculated with respect to **IM0** in kcal/mol)

#	dimer-anti	dimer-syn	Cy-anti	Cy-syn	RED	BLUE	bottom	top	R,R	S,S	ΔG‡_TS1	ΔG_IM3
1	1		1		1		1		1		38.3	18.9
2	1		1		1			1	1		36.3	11.9
3	1		1			1	1		1		38.0	15.0
4	1		1			1		1	1		37.2	18.6
5	1			1	1		1		1		47.9	27.6
6	1			1	1			1	1		22.7	1.8
7	1			1		1	1		1		26.8	4.8
8	1			1		1		1	1		47.5	23.1
9		1	1		1		1		1		41.9	23.5
10		**1**	**1**		**1**			**1**	**1**		**18.9**	**-2.2**
11		1	1			1	1		1		27.9	7.5
12		1	1			1		1	1		45.2	26.6
13		1		1	1		1		1		32.1	11.3
14		1		1	1			1	1		31.1	7.6
15		1		1		1	1		1		46.3	23.2
16		1		1		1		1	1		34.9	8.4
17	1		1		1		1			1	29.1	8.8
18	1		1		1			1		1	35.0	13.6
19	1		1			1	1			1	33.7	13.8
20	1		1			1		1		1	31.0	11.6
21	1			1	1		1			1	23.0	1.6
22	1			1	1			1		1	46.9	27.5
23	1			1		1	1			1	40.9	17.9
24	1			1		1		1		1	24.3	6.3
25		**1**	**1**		**1**		**1**			**1**	**22.8**	**2.5**
26		1	1		1			1		1	48.4	26.4
27		1	1			1	1			1	41.8	22.9
28		1	1			1		1		1	31.8	12.3
29		1		1	1		1			1	32.2	11.4
30		1		1	1			1		1	42.5	25.4
31		1		1		1	1			1	33.6	14.1
32		1		1		1		1		1	32.5	12.4

We also observed a good correlation between the activation free energy of **TS1** and that of **IM3**. Overall, the kinetically more favorable CHO ring opening transition state **TS1** would form a thermodynamically more stable Zn-alkoxide intermediate **ii**. This observation is in good agreement with the Hammond postulate.

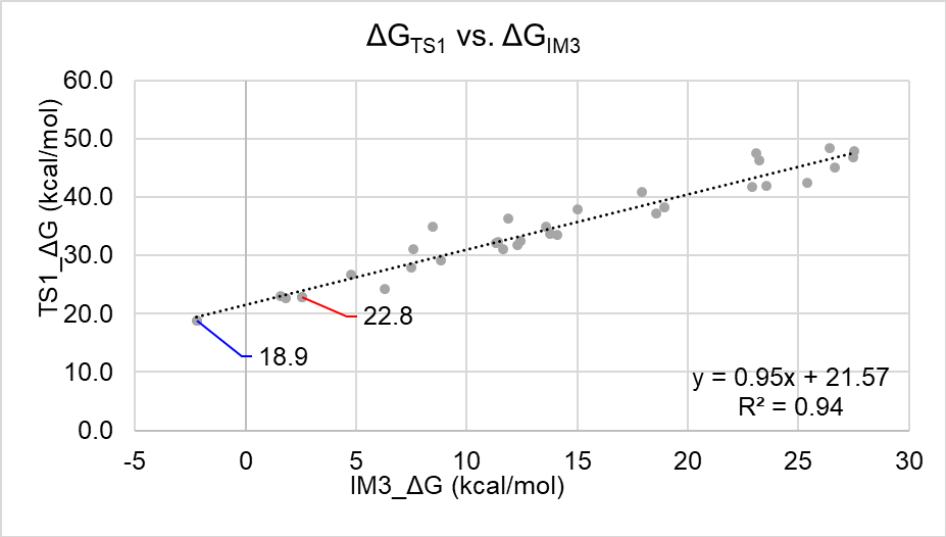

Figure S5. Correlation between ΔG‡ of **TS1** and ΔG of subsequent **IM3**

5. Less stable monomeric CHO insertion into Zn-acetate monomer of the initiation cycle

We have also calculated a potential monomeric CHO ring-opening transition state. Because **TS1_mono** is 35.0 kcal/mol higher in energy, with respect to **C1**, the monomeric CHO insertion is kinetically disfavored.

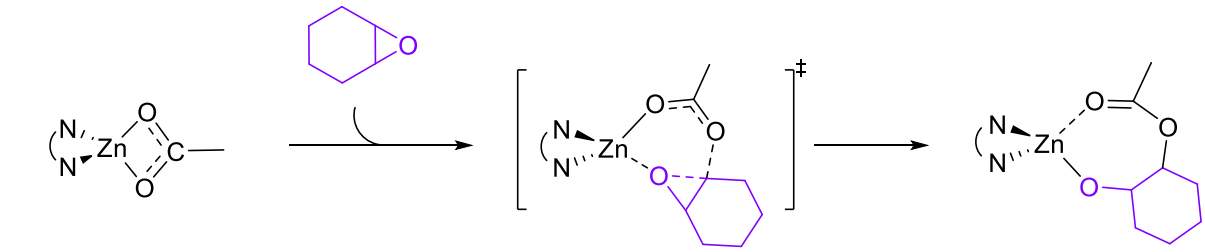

Figure S6. Correlation between ΔG‡ of **TS1** and ΔG of subsequent **IM6**

6. Scan of the CO_2 insertion (TS2) transition state reaction coordinate

Because we cannot locate the dimeric CO_2 insertion transition state after multiple attempts, we identified that the highest energy point along the reaction coordinate is at C-O distance at 1.90 Å (**Figure S7**). Scanning of the CO_2 insertion reaction coordinate is calculated at $SMD_{(toluene)}$/ M06 /6-311+G(d,p),SDD(Zn)//B3LYP-D3/6-31G(d),LANL2DZ(Zn) level of theory.

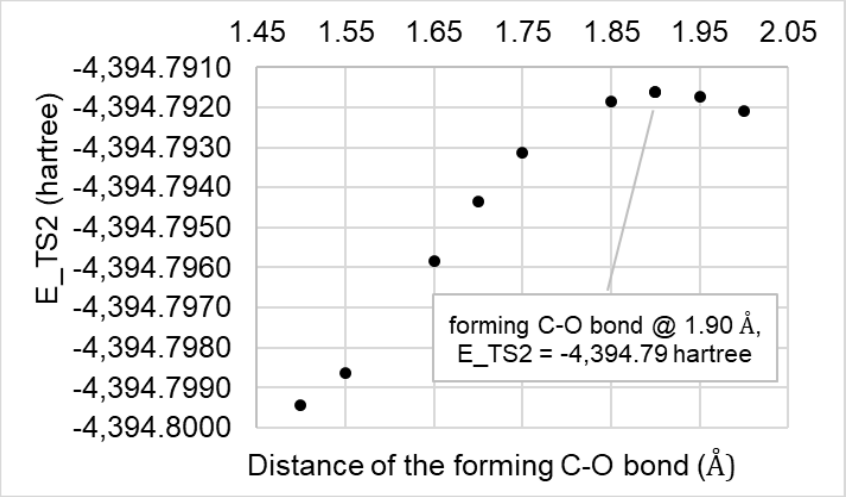

Figure S7. Scanned profile of the dimeric CO_2 insertion at $SMD_{(toluene)}$/ M06 /6-311+G(d,p),SDD(Zn)//B3LYP-D3/6-31G(d),LANL2DZ(Zn) level of theory

We then estimate the $\Delta G^{\ddagger}_{TS2}$ using a restrained modredundant calculation with C-O distance fixed at 1.90 Å**,** $SMD_{(toluene)}$/ ωB97XD /6-311+G(d,p),SDD(Zn)//B3LYP-D3/6-31G(d),LANL2DZ(Zn) level of theory, which is the same method used in all other calculations presented in the main manuscript.

7. Less stable conformations of the Zn-alkoxy monomer IM6

We identified a total of four conformations of the Zn-alkoxy monomer **IM6**. In the lowest energy conformation **IM6** is stabilized by the chelation of backbone acetate group with the CHO substrate closer to *N*-aryl group. In **IM6a** the CHO substrate locates closer to the N-cyclohexyl group, and is disfavored by 12.8 kcal/mol. In **IM6b**, OBn chelates the Zn(II) center and is disfavored by 9.3 kcal/mol. **IM6c** with no extra chelation is also disfavored by 7.1 kcal/mol.

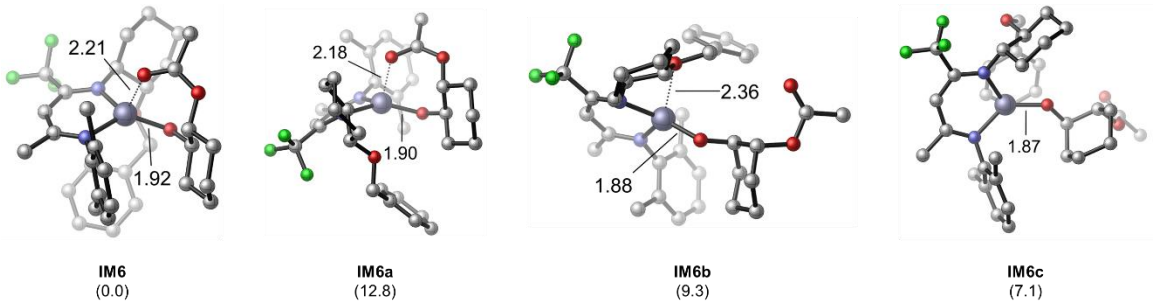

Figure S8. Conformations of **IM6** (ΔG in kcal/mol)

8. Less stable conformations of the monomeric CO_2 insertion transition state (TS3)

Figure **S9** presents a total of 8 conformations of the monomeric CO_2 insertion transition state of the cycle of initiation. All 7 conformations (**TS3a** to **TS3g**) are less stable than **TS3**, in which the acetate group at the end of the growing polymer chain chelates the Zn center, and the OBn substituent of the *N*-cyclohexyl group points toward the BDI backbone.

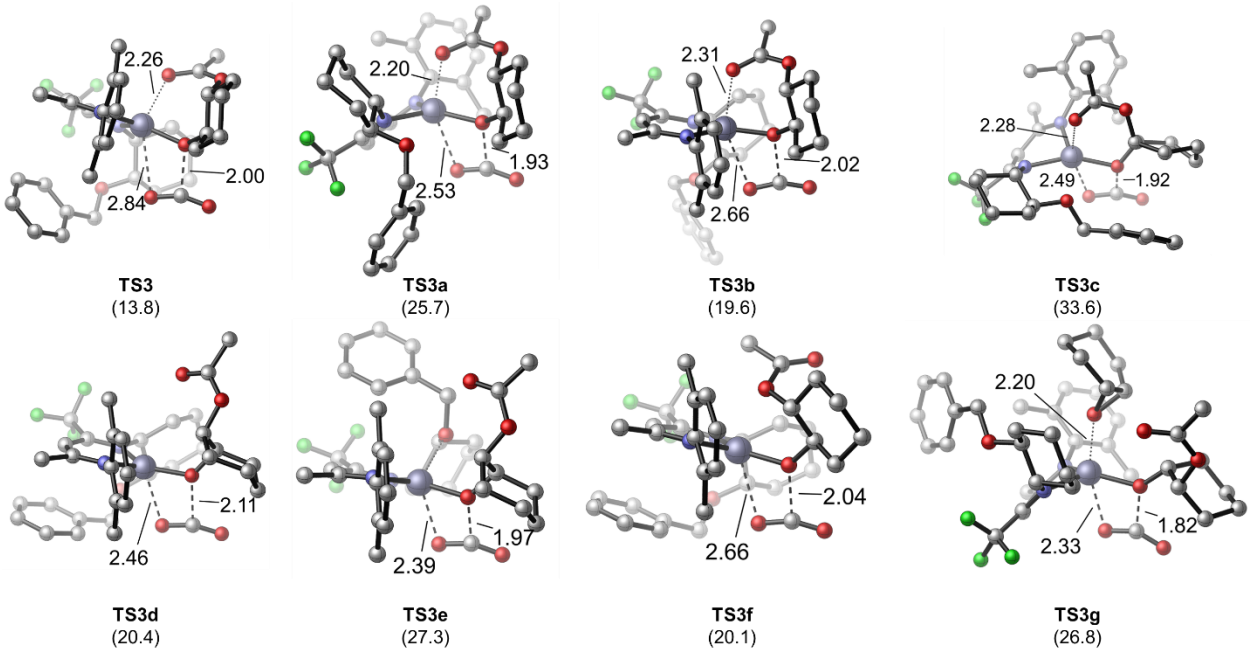

Figure S9. Conformations of **TS3** (ΔG in kcal/mol)

9. Procedure to calculate $\%V_{bur}$ for each quadrant

We calculate the $\%V_{bur}$ of the BDI ligand in each quadrant using the following procedure. Take the **TS1_*R,R*** as an example:

1) We first removed the CHO and inserting acetate group from the DFT optimized **TS1_*R,R***.
2) We then defined the cartesian coordinates using following procedure:
    a. The *x*-axis is defined as the line connecting the two Zn-atoms
    b. The origin is been set to the middle point of the line connecting the two Zn-atoms
    c. The *z*-axis is defined as the line connecting the origin and the carbon of the acetate group in the back.
    d. The *y*-axis is thus defined as the vertical line perpendicular to *x*- and *z*-axis
3) The $\%V_{bur}$ is then calculated using the SambVca 2.0[5] with following settings:
    a. The center of the sphere is set to the defined origin (middle point of the line connecting the two Zn-atoms)

b. The bondi radii is scaled by 1.17

c. The sphere radius is set to 5.0 Å

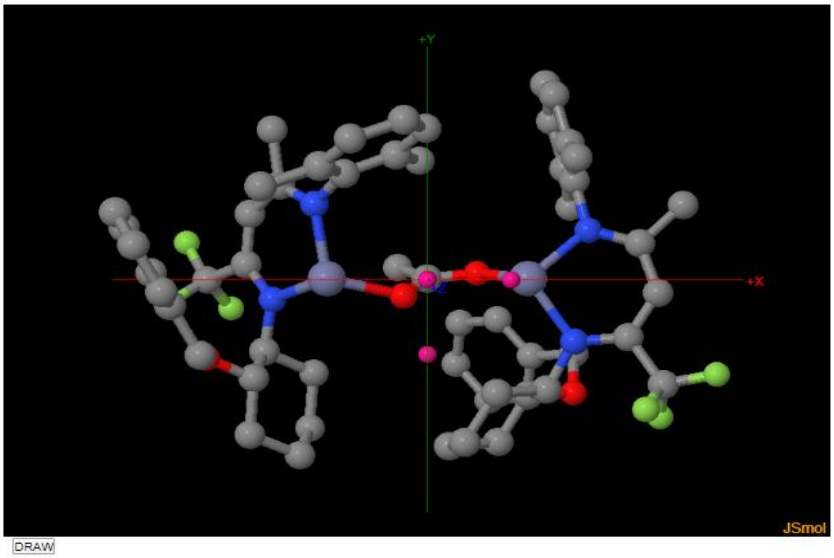

V Free	V Buried	V Total	V Exact
230.1	293.2	523.3	523.6

%V_Free	%V_Bur	% Tot/Ex
44.0	56.0	99.9

Quadrant	V_f	V_b	V_t	%V_f	%V_b
SW	77.6	53.2	130.8	59.3	40.7
NW	34.3	96.5	130.8	26.2	73.8
NE	56.0	74.8	130.8	42.8	57.2
SE	62.1	68.7	130.8	47.5	52.5

Figure S10. Procedure to calculate $\%V_{bur}$ of BDI ligand in TS1_*R,R*

10. Procedure to calculate the dispersive interaction energy between the substrates and the BDI ligand in each quadrant

We calculated the dispersive interaction energy between the substrates and the BDI ligand in each quadrant using the following procedure. **Figure S11** depicts the procedure to calculate the dispersive interaction energy between the substrate and the Ar^1 of the BDI ligand in **TS1_*R,R***. The dispersion energy is calculated using the DFTD3 program.

1) We first calculated the dispersive interaction of Ar^1 in Q1 with rest of the molecule:
   a. total dispersion energy in the DFT optimized structure of **TS1_*R,R*** is E_{disp_total}
   b. After replacing the Ar^1 with a hydrogen, we calculated the total dispersion energy again ($E_{disp\_total\_noQ1}$)
   c. As such, the difference between E_{disp_total} and $E_{disp\_total\_noQ1}$ is the contribution of Q1 to the total dispersive interactions (E_{disp_Q1})

2) We then calculate the dispersive interaction of Ar^1 in Q1 with the other BDI ligand only:
    a. We first removed both Zn atoms, both acetate groups, and the CHO substrate
    b. Then we calculated the total dispersion energy between the two BDI ligands, which is $E_{disp\_total\_ligand}$
    c. Then we replaced the Ar^1 with a hydrogen and calculated the $E_{disp\_total\_ligand\_noQ1}$
    d. The difference between $E_{disp\_total\_ligand}$ and $E_{disp\_total\_ligand\_noQ1}$ is the contribution of Q1 to the dispersive interactions between the ligands ($E_{disp\_ligand\_Q1}$)
3) By taking the difference between E_{disp_Q1} and $E_{disp\_ligand\_Q1}$, we can calculate the dispersive interaction between the *N*-Ar^1 group and the substrates (both acetates and the CHO) $E_{disp\_sub\_Q1}$ in **TS1_*R,R***.

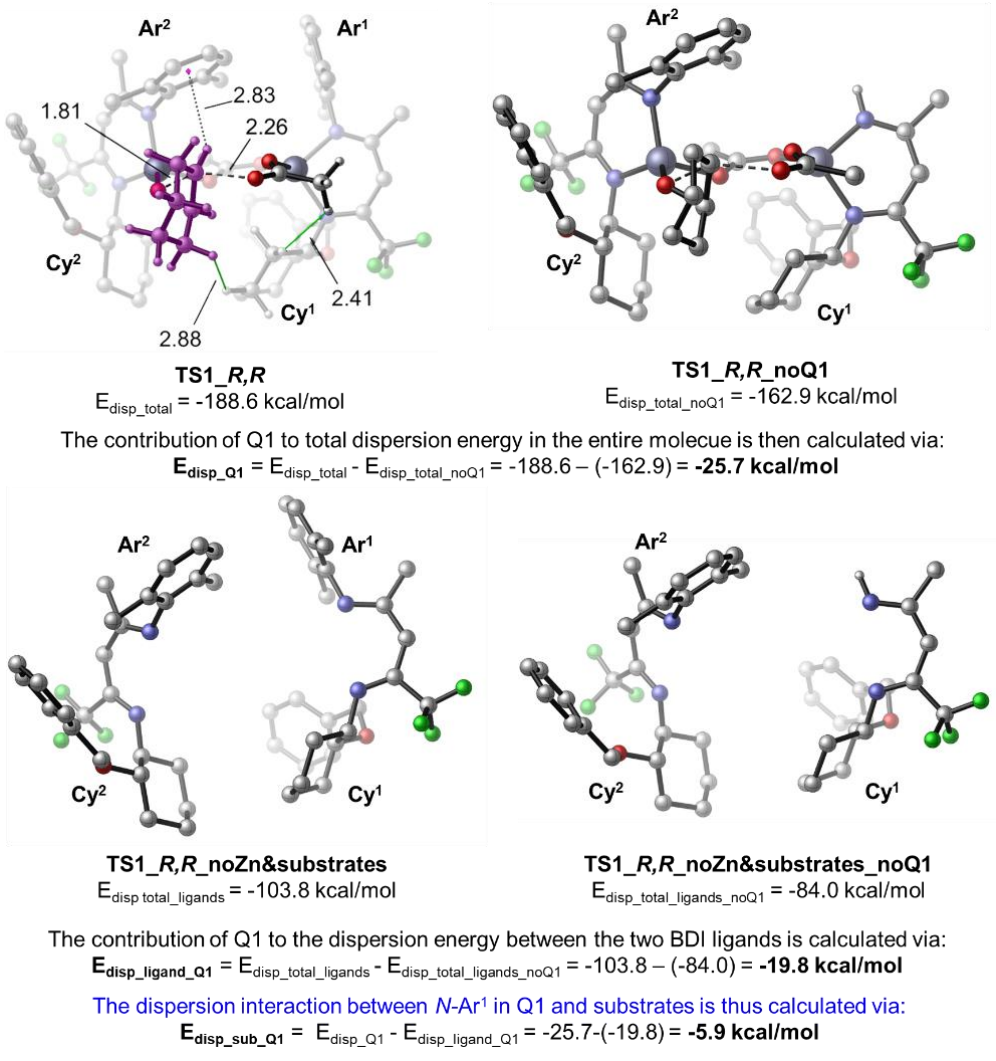

Figure S11. Procedure to calculate dispersive interaction energy between the substrate and the Ar^1 of the BDI ligand in **TS1_*R,R***

11. Less favorable competing pathways along the cycle of propagation with C1

We have also considered the two possible competing pathways from the Zn-alkoxy/Zn-carbonate mixed dimer **IM12**. The free energy of activation of a dimeric CO_2 insertion is estimated from restrained calculation by fixing the forming C-O bond at 2.00 Å. The high kinetic energy barriers of **TS2_propagation** and **TS1b_propagation** suggest neither pathways are operative along the cycle of propagation with **C1**.

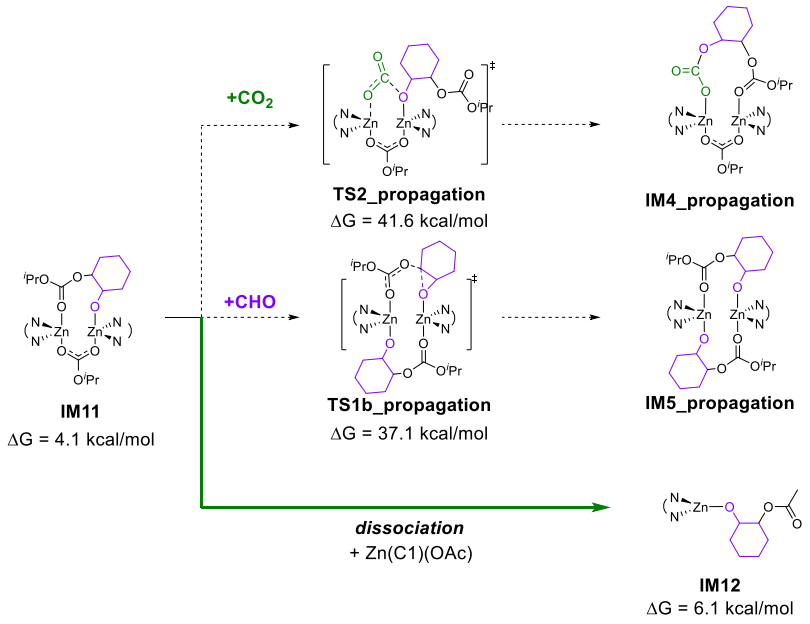

Figure S12. Higher energy competing pathways along the cycle of propagation

Because we cannot locate the dimeric CO_2 insertion transition state in the propagation cycle after multiple attempts, we identified that the highest energy point along the reaction coordinate is at C-O distance at 2.00 Å (**Figure S13**). Scanning of the CO_2 insertion reaction coordinate is calculated at $SMD_{(toluene)}$/ ωB97XD /6-311+G(d,p),SDD(Zn)//B3LYP-D3/6-31G(d),LANL2DZ(Zn) level of theory. We then calculated the frequencies using a restrained modredundant calculation with C-O distance fixed at 2.00 Å, at B3LYP-D3/6-31G(d),LANL2DZ(Zn) level of theory, which is the same method used in all other calculations presented in the main manuscript.

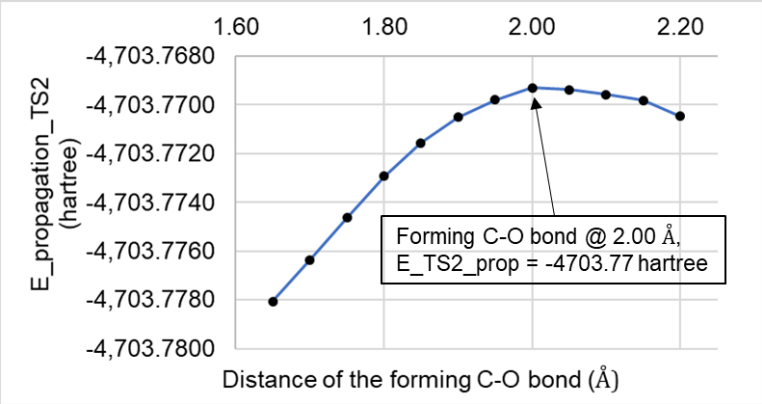

Figure S13. Scanned profile of TS2_propagation at $SMD_{(toluene)}$/ ωB97XD /6-311+G(d,p),SDD(Zn)//B3LYP-D3/6-31G(d),LANL2DZ(Zn) level of theory

12. Effects of BDI backbone and *N*-Cy substitution on the rate- and enantioselectivity

The computed ΔG‡ for BDI ligand backbone substituted catalysts (**C12**-**C17**) are almost similar or higher than that with the **C1** catalyst. Among the series, **C13** and **C14** slightly improve the enantioselectivity, the calculated reactivity is much lower than the parent **C1** catalyst. As such, we concluded that modification of the BDI ligand backbone does not further improve the reactivity nor enantioselectivity as compared with catalyst **C1**.

Table S3. Effects of electronically and sterically distinct backbone substituents of the BDI ligand on the rate and enantioselectivity of the initiation cycle of CHO/CO2 copolymerization reaction

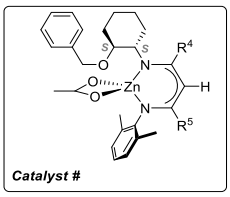

catalyst	R^4 =	R^5 =	$\Delta G^{\ddagger}_{R,R}$	$\Delta G^{\ddagger}_{S,S}$	$\Delta\Delta G^{\ddagger}$
C12	CF_3	CF_3	19.0	23.1	4.1
C13	CH_3	CF_3	22.8	26.2	5.1
C14	CH_3	CH_3	22.7	26.3	5.4
C15	CF_3	Et	22.8	25.1	3.5
C16	CF_3	iPr	24.1	26.8	4.0
C17	CF_3	OMe	23.2	26.0	3.6

**All energies in kcal/mol*

We studied **C18** (with C_6F_5 substituent instead of OBn on the *N*-cyclohexyl group) catalyzed CHO/CO_2 copolymerization reaction. The calculated $\Delta G^{\ddagger}_{R,R\_C18}$ = 15.9 kcal/mol and $\Delta G^{\ddagger}_{S,S\_C18}$ = 19.6 kcal/mol. As such, **C18** is predicted to show very similar enantioselectivity and higher reactivity of CHO/CO_2 copolymerization reaction as compared with catalyst **C1** ($\Delta G^{\ddagger}_{R,R\_C1}$ = 18.9 kcal/mol and $\Delta G^{\ddagger}_{S,S\_C1}$ = 22.8 kcal/mol).

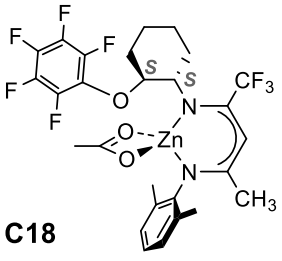

C18

13. PES of the cycle of initiation of C10-catalyzed CHO/CO_2 copolymerization reaction

The **C10**-catalyzed CHO/CO_2 copolymerization reaction proceeds via the same mixed reaction mechanism. The dimeric CHO ring-opening (**TS1**) is the rate- and enantioselectivity determining step of the cycle of initiation.

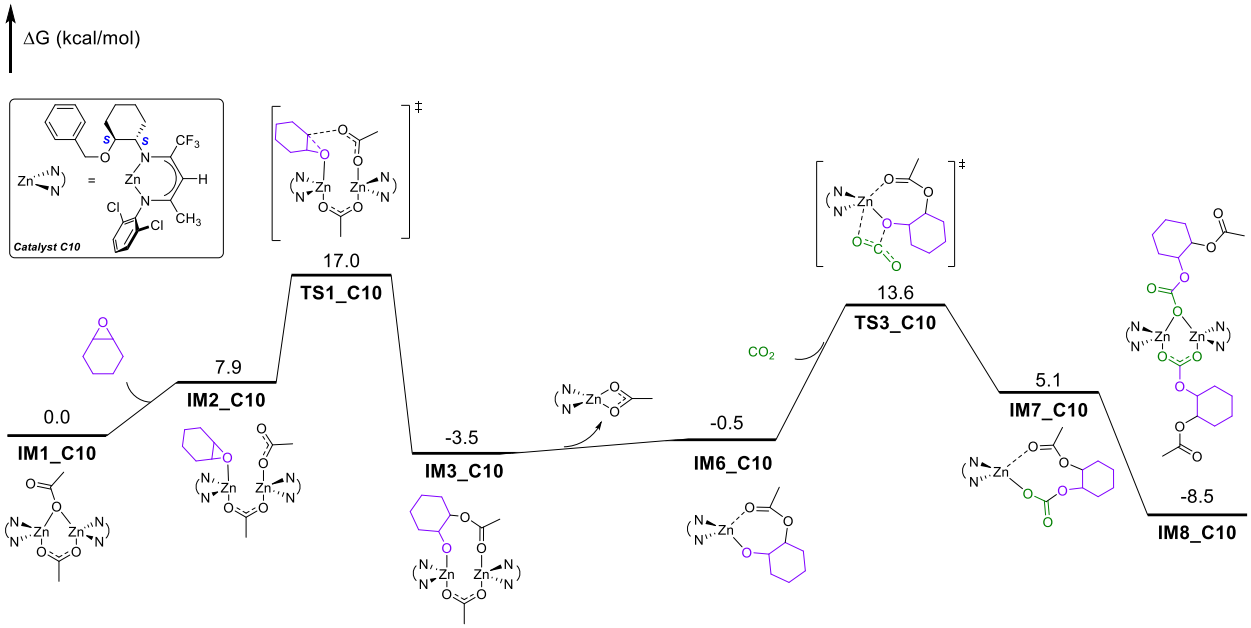

Figure S14. Computed potential energy surface of the initiation cycle of the **C10**-catalyzed CO_2/CHO copolymerization reaction

14. PES of the cycle of initiation of C19-catalyzed CHO/CO_2 copolymerization reaction

In 2003, Coates group reported catalyst **C19** to be an active catalyst for CHO/CO_2 copolymerization reaction to produce high % carbonate linkages and good TOF.[6] Figure S15 summarized the computed PES of the initiation mechanism of the **C19**-catalyzed CHO/CO_2 copolymerization reaction. The **C19**-catalyzed CHO/CO_2 copolymerization reaction proceeds via the same mixed reaction mechanism. Because the dimeric CHO ring-opening (**TS1_C19**) requires higher free energy of activation (24.8 kcal/mol) than the monomeric CO_2 insertion (**TS3_C19**), (21.1 kcal/mol), we conclude that the **TS1_C19** is the rate-limiting step of the cycle of initiation with the C2 symmetric catalyst **C19**.

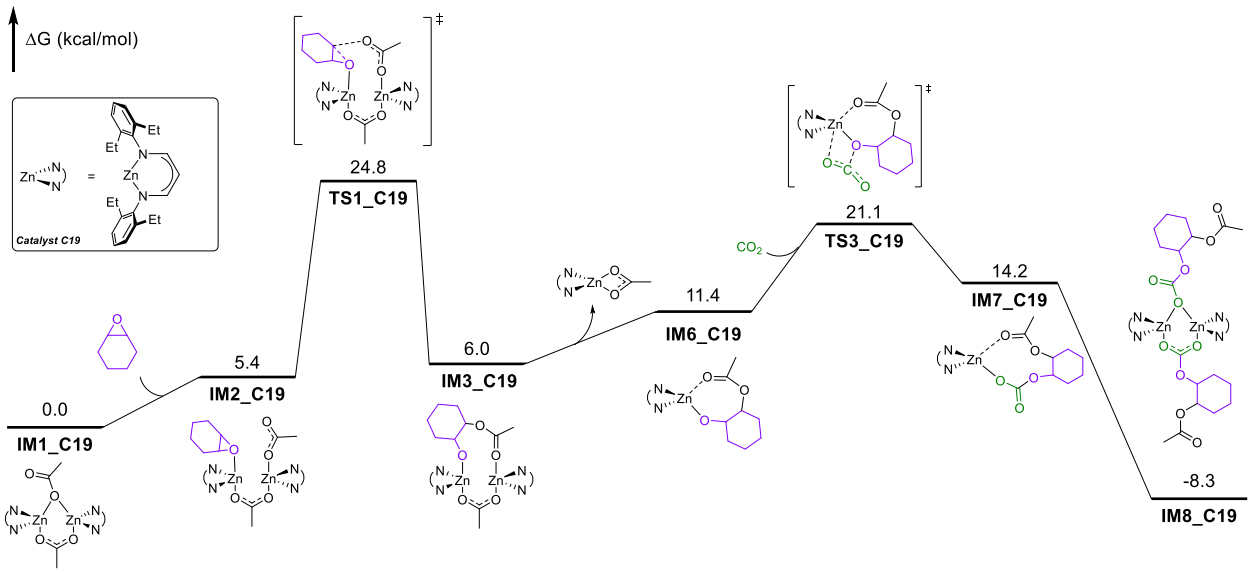

Figure S15. Computed potential energy surface of the initiation cycle of the **C19**-catalyzed CO_2/CHO copolymerization reaction

15. Energies of all structures in main article

Main-Article	E	ZPE	H	T.S	T.qh-S	G(T)	qh-G(T)	E_sol-wb97
**********								
CO2	-188.582581	0.011592	-188.567397	0.02431	0.02431	-188.591707	-188.591707	-188.580822
R_S_Epoxide	-309.875843	0.152634	-309.716323	0.036424	0.036422	-309.752746	-309.752745	-309.848822
IM1	-3574.882217	1.14363	-3573.661739	0.194332	0.182427	-3573.856071	-3573.844166	-3897.629508
IM2	-3884.768248	1.298609	-3883.385448	0.209835	0.19682	-3883.595283	-3883.582268	-4207.490925
TS1	-3884.755698	1.297975	-3883.37422	0.20732	0.194822	-3883.58154	-3883.569043	-4207.473712
IM3	-3884.791745	1.301669	-3883.407291	0.204274	0.192747	-3883.611565	-3883.600039	-4207.512413
TS2	-4073.352941	1.31285	-4071.95376	0.215479	0.201317	-4072.169238	-4072.155076	-4396.06103
IM4	-4073.405354	1.316501	-4072.002857	0.211865	0.20005	-4072.214722	-4072.202907	-4396.113694
TS1b	-4194.635432	1.454262	-4193.091084	0.221761	0.207802	-4193.312845	-4193.298886	-4517.325529
IM5	-4194.686121	1.458101	-4193.13855	0.219368	0.205997	-4193.357918	-4193.344546	-4517.37956
IM6	-2097.326711	0.727626	-2096.554537	0.121512	0.116559	-2096.676049	-2096.671096	-2258.677025
TS3	-2285.913058	0.740696	-2285.124812	0.128977	0.123139	-2285.253789	-2285.247951	-2447.254551
IM7	-2285.930599	0.743555	-2285.140046	0.12699	0.121479	-2285.267036	-2285.261524	-2447.270461
IM8	-4571.928264	1.489113	-4570.343807	0.232432	0.218266	-4570.576238	-4570.562072	-4894.602378
TS1_SS	-3884.754773	1.298672	-3883.373001	0.204939	0.193472	-3883.57794	-3883.566473	-4207.469146
IM9	-3882.636124	1.268547	-3881.284042	0.20653	0.194985	-3881.490573	-3881.479027	-4205.361068
IM10	-4192.531506	1.423118	-4191.017328	0.223013	0.209841	-4191.240341	-4191.227169	-4515.223922
TS4_R_R	-4192.506623	1.422242	-4190.994008	0.221112	0.208168	-4191.21512	-4191.202176	-4515.196502
TS4_S_S	-4192.50701	1.423032	-4190.993827	0.219852	0.20738	-4191.213679	-4191.201207	-4515.194937
IM11_R_R	-4192.537517	1.426193	-4191.021594	0.218688	0.20637	-4191.240283	-4191.227964	-4515.232788
IM12	-2251.19394	0.789919	-2250.356049	0.128904	0.123209	-2250.484953	-2250.479257	-2412.532688
TS5	-2439.780757	0.803147	-2438.926735	0.136134	0.129563	-2439.062869	-2439.056298	-2601.110526
IM13	-2439.800834	0.805667	-2438.944618	0.135132	0.128723	-2439.079751	-2439.073342	-2601.130163
IM14	-4879.666399	1.613403	-4877.95062	0.249347	0.232423	-4878.199967	-4878.183044	-5202.319076
IM1_C2	-3574.880889	1.14267	-3573.660636	0.198732	0.184776	-3573.859368	-3573.845412	-3897.625147
TS1_RR_C2	-3884.75635	1.296931	-3883.37524	0.21026	0.19671	-3883.5855	-3883.57195	-4207.465677
TS1_SS_C2	-3884.759401	1.298021	-3883.377932	0.205923	0.194255	-3883.583854	-3883.572187	-4207.469329
IM1_C3_real	-3417.586201	1.03254	-3416.483801	0.179855	0.168711	-3416.663656	-3416.652511	-3740.355713
TS1_RR_C3	-3727.459635	1.185723	-3726.197692	0.19164	0.180501	-3726.389332	-3726.378193	-4050.194733
TS1_SS_C3	-3727.462498	1.186935	-3726.199133	0.191294	0.180594	-3726.390427	-3726.379727	-4050.196367
IM1_C4	-4765.75522	1.051021	-4764.619875	0.211172	0.197703	-4764.831047	-4764.817578	-5088.568159
TS1_RR_C4	-5075.62729	1.205328	-5074.330874	0.226052	0.210413	-5074.556927	-5074.541288	-5398.408787
TS1_SS_C4	-5075.625129	1.205826	-5074.328739	0.22137	0.208148	-5074.550109	-5074.536888	-5398.405027
IM1_C5	-3732.157979	1.259816	-3730.816402	0.204477	0.192039	-3731.020879	-3731.008441	-4054.88633
TS1_RR_C5	-4042.030323	1.414141	-4040.527631	0.21916	0.205037	-4040.746791	-4040.732668	-4364.72908
TS1_SS_C5	-4042.027119	1.41459	-4040.524263	0.217778	0.204199	-4040.742041	-4040.728461	-4364.721598
IM1_C6	-3889.438735	1.374314	-3887.977616	0.212215	0.200581	-3888.189832	-3888.178198	-4212.147036
TS1_RR_C6	-4199.304518	1.528917	-4197.680616	0.231185	0.216511	-4197.911801	-4197.897127	-4521.981339
TS1_SS_C6	-4199.297252	1.528887	-4197.67507	0.225675	0.212754	-4197.900745	-4197.887824	-4521.974003
IM1_C7	-3814.515522	0.999743	-3813.442523	0.186305	0.174667	-3813.628828	-3813.61719	-4137.303669
TS1_RR_C7	-4124.392522	1.153885	-4123.158618	0.199084	0.187603	-4123.357702	-4123.34622	-4447.15082
TS1_SS_C7	-4124.391274	1.153856	-4123.157586	0.198118	0.186868	-4123.355705	-4123.344454	-4447.147109
IM1_C8	-4012.975915	0.983221	-4011.917606	0.190944	0.178383	-4012.108549	-4012.095989	-4335.780221
TS1_RR_C8	-4322.853652	1.137339	-4321.634452	0.203507	0.19118	-4321.837959	-4321.825632	-4645.628264
TS1_SS_C8	-4322.852957	1.137355	-4321.633993	0.202089	0.190338	-4321.836082	-4321.824331	-4645.624129
IM1_C9	-4409.846616	0.950053	-4408.817089	0.200408	0.187261	-4409.017497	-4409.00435	-4732.679808
TS1_RR_C9	-4719.726513	1.104813	-4718.536022	0.209633	0.198035	-4718.745655	-4718.734057	-5042.527309
TS1_SS_C9	-4719.726667	1.104407	-4718.536578	0.20966	0.197911	-4718.746238	-4718.734488	-5042.524576
IM1_C10	-5255.960909	0.992374	-5254.893121	0.195205	0.180685	-5255.088326	-5255.073806	-5578.778328
TS1_RR_C10	-5565.842758	1.147619	-5564.613351	0.204716	0.192128	-5564.818067	-5564.805479	-5888.627164
TS1_SS_C10	-5565.838727	1.147786	-5564.609427	0.202798	0.1911	-5564.812225	-5564.800528	-5888.619502
IM1_C11	-13700.81917	0.990806	-13699.75199	0.19803	0.183451	-13699.95002	-13699.93544	-14034.64024
TS1_RR_C11	-14010.70396	1.146301	-14009.47504	0.207974	0.194588	-14009.68302	-14009.66963	-14344.48814
TS1_SS_C11	-14010.69877	1.146185	-14009.47012	0.206534	0.193839	-14009.67665	-14009.66396	-14344.47975
IM9_dCl	-5563.716329	1.117461	-5562.516654	0.207166	0.193709	-5562.723819	-5562.710363	-5886.510649
TS4_R_R_dCl	-5873.597247	1.271788	-5872.236885	0.217765	0.205	-5872.454651	-5872.441885	-6196.35298
TS4_S_S_dCl	-5873.589758	1.271482	-5872.229281	0.22019	0.206173	-5872.44947	-5872.435454	-6196.346351

*All energies in this table are in hatree

References:

(1) Zhao, Y.; Truhlar, D. G. The M06 suite of density function-als for main group thermochemistry, thermochemical kinet-ics, noncovalent interactions, excited states, and transition elements: two new functionals and systematic testing of four M06-class functionals and 12 other functionals. *Theor. Chem. Acc.,* **2008**. *120*. 215-241

(2) Haoyu, S. Y.; He, X.; Li, S. L.; Truhlar, D.G. MN15: A Kohn–Sham global-hybrid exchange–correlation density functional with broad accuracy for multi-reference and single-reference systems and noncovalent interactions. *Chem. Sci.,* **2016**. *7,* 5032-5051.

(3) Schäfer, A.; Horn, H.; Ahlrichs, R. Fully optimized contracted Gaussian basis sets for atoms Li to Kr. *J. Chem. Phys.,* **1992**. *97*, 2571-2577

(4) Ellis, W. C.; Jung, Y.; Mulzer, M.; Di Girolamo, R.; Lobkovsky, E. B.; Coates, G. W. Copolymerization of CO 2 and meso epoxides using enantioselective β-diiminate catalysts: a route to highly isotactic polycarbonates. *Chem. Sci.*, **2014**. *5*, 4004-4011.

(5) Falivene, L.; Credendino, R.; Poater, A.; Petta, A.; Serra, L.; Oliva, R.; Scarano, V.; Cavallo, L. SambVca 2. A web tool for analyzing catalytic pockets with topographic steric maps. *Organometallics,* **2016**. *35*, 2286-2293.

(6) Moore, D.R.; Cheng, M.; Lobkovsky, E.B.; Coates, G.W. Mechanism of the alternating copolymerization of epoxides and CO2 using β-diiminate zinc catalysts: evidence for a bimetallic epoxide enchainment. *J. Am. Chem. Soc*, **2003**. *125(39),* 11911-11924.